J. Fluid Mech. (2001), *vol.* 442, *pp.* 119–140. Printed in the United Kingdom

Direct numerical simulation of instabilities in a two-dimensional near-critical fluid layer heated from below

By S. AMIROUDINE[1,2], P. BONTOUX[1]†, P. LARROUDÉ[1,3], B. GILLY[1] AND B. ZAPPOLI[4]

[1]Laboratoire de Modélisation et Simulation Numérique en Mécanique, IMT-Château-Gombert, CNRS, Université d'Aix-Marseille II, 38, rue Frédéric Joliot-Curie, 13451 Marseille Cedex 20, France

[2]Département de Physique, Université des Antilles-Guyane, Faculté des Sciences, 917159 Pointe-a-Pitre Cedex, Guadeloupe, France

[3]LEGI, CNRS, Université Joseph Fourier, BP 53, 38041 Grenoble Cedex, France

[4]CNES/DP/MP/SC, 18 Av. Edouard Belin, 31401 Toulouse Cedex 04, France

(Received 22 December 1998 and in revised form 18 December 2000)

An analysis of the hydrodynamic stability of a fluid near its near critical point – initially at rest and in thermodynamic equilibrium – is considered in the Rayleigh–Bénard configuration, i.e. heated from below. The geometry is a two-dimensional square cavity and the top and bottom walls are maintained at constant temperatures while the sidewalls are insulated. Owing to the homogeneous thermo-acoustic heating (piston effect), the thermal field exhibits a very specific structure in the vertical direction. A very thin hot thermal boundary layer is formed at the bottom, then a homogeneously heated bulk settles in the core at a lower temperature; at the top, a cooler boundary layer forms in order to continuously match the bulk temperature with the colder temperature of the upper wall. We analyse the stability of the two boundary layers by numerically solving the Navier–Stokes equations appropriate for a van der Waals' gas slightly above its critical point. A finite-volume method is used together with an acoustic filtering procedure. The onset of the instabilities in the two different layers is discussed with respect to the results of the theoretical stability analyses available in the literature and stability diagrams are derived. By accounting for the piston effect the present results can be put within the framework of the stability analysis of Gitterman and Steinberg for a single layer subjected to a uniform, steady temperature gradient.

1. Introduction

Interest in the hydrodynamics of supercritical fluids dates from the early 1990s. Reputed physicists reported what they termed a fourth heat equilibration mechanism from experiments in free convection. The phenomenon was particularly obvious in pure fluid layers near critical conditions and was termed as the 'piston effect' (PE). This thermo-acoustic effect, which was predicted theoretically (Boukari *et al.* 1990; Onuki, Hao & Ferrel 1990; Zappoli *et al.* 1990; Zappoli 1992; Carlès 1995; Zhong & Meyer 1995) after an experimental observation by Nitsche & Straub (1987), is

† Author to whom correspondence should be addressed.

responsible for fast thermal equilibration in the absence of convection and conduction. It was then explored experimentally for micro-gravity conditions that suppress the convective component of the heat transport (Guenoun *et al.* 1993; Garrabos *et al.* 1998). Numerical modelling has confirmed and has contributed to the understanding of the hydrodynamics of these very compressible, low heat diffusing, dense fluids (Bravais, Zappoli & Mignon 1993; Zappoli & Durand-Daubin 1994; Amiroudine 1995; Amiroudine *et al.* 1996; Larroudé *et al.* 1996; Zappoli *et al.* 1996). The question which then naturally arose was that of heat transport in near-critical fluids under conditions of terrestrial gravity, or, more specifically, the interaction between the PE and natural convection.

The problem is complex and broad since it addresses the hydrodynamics of hyper-compressible, low-heat diffusing pure fluids. The fluids are characterized by a high density (close to the density of the liquid) and by a low viscosity (close to the viscosity of the gas). The heat transfer is governed by a very large compressibility and by a vanishing thermal diffusivity. Some recent numerical simulations and experiments have shown that the interaction of the PE with convection depends on the boundary conditions. In order to avoid hydrodynamic stability issues, Zappoli *et al.* (1996) considered a two-dimensional square cavity filled with a near-critical fluid subjected to heating along a vertical boundary, the three other walls being thermally insulated. The result was the striking evidence of the existence of a quasi-isothermal convective motion of the fluid; the PE generated along the vertical heated wall equilibrates the bulk temperature on a time scale shorter than that required to initiate convection. Convection is then triggered by the remaining vanishing thermal inhomogenities that still provoke large density gradients orthogonal to the gravity vector, owing to the large compressibility of the fluid. This result seemed to contradict the experimental observations of Garrabos *et al.* (1998) who reported a decrease of the adiabatic heating (PE) when heated by a thermistor in the presence of convection. Further numerical simulations taking into account the thermal interaction with boundaries (Zappoli *et al.* 1999) showed that the decrease of the bulk temperature came from a homogeneous, bulk PE triggered by the thermal plume rising from the thermistor impinging on the upper constant-temperature wall.

The continuation of these studies led us naturally to consider the Rayleigh–Bénard configuration, i.e. a fluid layer heated from below. In such a case, internal motion begins within the fluid (free convection), attempting to even out the temperature in the whole volume of fluid by thermal expansion. However, this motion is hindered by the density and the pressure stratification in the fluid and dissipative processes. When considered separately, one or other of these two factors lead to the two well-known stability criteria due to Schwarzchild and Rayleigh (Normand, Pomeau & Velarde 1977) for determining the onset of convection. The Boussinesq equations in which density variations are neglected except in the term describing the buoyancy driving force are equally applicable to compressible fluids; in such a case, an equivalent compressible Rayleigh number can be derived (Spiegel 1965). In the case of near-critical fluids, the volume expansion coefficient diverges which suggests that the convective instabilities become more and more important. Gitterman & Steinberg (1970*a,b*) derived the convection threshold in the classical Rayleigh–Bénard problem for fluids near the critical point, by heuristic arguments. Recent experimental investigations of Rayleigh–Bénard convection near the critical condition are reported in Assenheimer & Steinberg (1993) and by Kogan, Murphy & Meyer (1999) for SF_6 and ^3He gases, respectively.

However, the present situation, in which the fluid is at rest and in thermodynamic

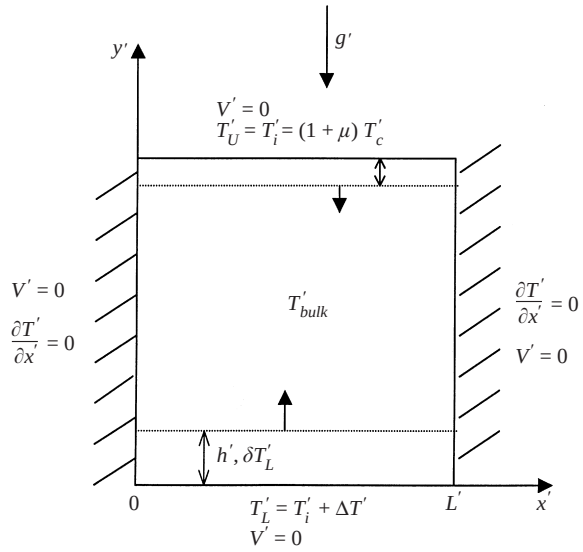

FIGURE 1. Geometry of the square cavity of height $L' = 10\,\text{mm}$ with horizontal axis x' and vertical axis y' which is co-linear with the acceleration due to gravity g'. Velocity and temperature boundary conditions at the walls. Characteristic zones: isothermal bulk in the core, hot and cold layers near the two bottom and top horizontal walls. The directions and the senses of the expansion with time of these layers in the core are visualized by the arrows and they are characterized by the local height h' and by the local temperature differences, $\delta T'_L$ in the hot layer.

equilibrium, is more complex. The bulk is homogeneously heated by the piston effect and a cold boundary layer thus forms along the top wall. Thus, the problem under consideration here involves more than the bottom-heated boundary layer topped by the bulk phase at the initial temperature, as is the case in classical configurations with compressible fluids. The hydrodynamic stability of this configuration thus depends on the stability of two layers which leads us to address two different stability problems: the first for the bottom-heated layer and the second for the top-cooled one, the two being separated by a thermally uniform bulk at an intermediate temperature. The numerical prediction of the stability threshold is performed and discussed in the present paper. The estimate of the local Rayleigh number shows that, provided the relevant lengthscales and temperature differences (due to the piston effect) are taken into account, the Gitterman & Steinberg stability criterion, applied to either one of the layers, works well in predicting the thresholds.

In § 2, the modelling is presented. In § 3 we consider the different analyses which address the onset of convection. The approach to the present stability analysis is introduced and discussed in § 4. The numerical method is briefly recalled in § 5, together with the details on the numerical simulation. The physical phenomena and the results are presented and discussed in § 6.

2. The mode1

The same model as developed in Amiroudine (1995) and Zappoli *et al.* (1996) has been used in the analysis of Rayleigh–Bénard convection. We consider a two-dimensional square cavity of height $L' = 10\,\text{mm}$ heated from below, with insulated vertical walls subjected to a gravitational field. The configuration is shown in figure 1. Horizontal and vertical directions are denoted by x' and y', respectively. The stratified

fluid is initially at rest in thermodynamic equilibrium such that:

$$\frac{T_i' - T_c'}{T_c'} = \mu \ll 1,$$

where T_i' and T_c' are the initial and critical temperatures, respectively, and primes denote dimensional variables; the parameter μ defines the dimensionless proximity to the critical point. The domain is initially at uniform temperature T_i' and a temperature increase $\Delta T'$ is applied at the bottom of the cavity (some mK per second). The top wall is maintained at the initial temperature ($T_U' = T_i'$). In our numerical simulations, both solid boundaries are initially at the same temperature T_i' and the bottom wall undergoes a change in temperature $T_L' = T_i' + \Delta T'$. This procedure avoids strong initial discontinuities.

The governing Navier–Stokes equations are those of a Newtonian, viscous, hypercompressible, heat-conducting van der Waals' gas (Zappoli *et al.* 1996). The fluid is not too close to the critical point so that the hypothesis of a continuous medium remains valid. According to Assenheimer & Steinberg (1996), the hydrodynamic limit is around $\mu \approx 10^{-6}$, which corresponds to $T_i' - T_c' \approx 0.3\,\mathrm{mK}$ for CO_2. Here, we consider $T_i' - T_c' \approx 1\,\mathrm{K}$. We have chosen the van der Waals' equation as the equation of state. This choice results from a compromise between the reliability of the description and the computational time; the use of real gas data would significantly increase the computational time, but would also require substantially more intricate algorithms. As the pressure appears in the form of a gradient (in the momentum equation), the result does not depend on its initial background value, which is why we consider the two critical coordinates to be density and temperature and use the van der Waals' equation. Concerning the divergence of the isothermal compressibility, the model of van der Waals gives a μ^{-1} behaviour whereas the real dependence is $\mu^{-1.24}$. As the initial conditions are, at present, not taken too close to the critical point (1 K higher), we consider that the van der Waals' equation leads to the correct phenomenology (as we did in previous papers on near-critical fluid hydrodynamics (Zappoli 1996, 1997). To explore closer to the critical point or to compare the obtained thermal field with specific experiments, we would certainly do better with the cubic equation of Moldover *et al.* (1979) at the expense of a significant lengthening of the computation time. The following transport coefficients are considered:

$$\lambda = \frac{\lambda'}{\lambda_0'} = 1 + \Lambda \left(\frac{T' - T_c'}{T_c'} \right)^{-0.5}, \quad C_v = \frac{C_v'}{C_{v0}'} = 1, \quad \eta = \frac{\eta'}{\eta_0'} = 1,$$

where λ', C_v' and η' are the thermal conductivity (in which $\Lambda = 0.75$), the heat capacity at constant volume and the molecular viscosity, respectively; the subscript 0 represents the value far from the critical point. The heat capacity at constant volume and the viscosity have been considered as constant and equal to the value for gaseous CO_2 considered as an ideal gas.

The equations are made dimensionless, as in Zappoli *et al.* (1996). The density and the temperature are scaled relative to their critical values ρ_c' and T_c', respectively, $\rho_c' = 467.8\,\mathrm{kg\,m^{-3}}$ and $T_c' = 304.13\,\mathrm{K}$, and the pressure with respect to its perfect gas value, i.e. $\rho_c' R' T_c'$ ($R' = 188.8\,\mathrm{J\,kg^{-1}\,K^{-1}}$). Since the problem is to investigate the interaction between the PE and buoyant convection following a change in boundary temperature, the characteristic timescale should be the shorter of the two effects. Even if these two-dimensional timescales are of the same order at a few degrees K from

the critical point, the PE timescale will be much shorter as we approach it. The latter is thus taken as the characteristic time.

The following non-dimensional PE velocity and time are used (Zappoli 1992; Zappoli *et al.* 1996): $\boldsymbol{V}_\tau = \boldsymbol{V}/c_\tau$, $\tau = c_\tau t$ with $c_\tau = \varepsilon f(\mu, \Lambda)/\mu^2$ and $f(\mu, \Lambda) = \mu((1/\Lambda) + (1/\mu^{1/2}))$. Here, $\boldsymbol{V}$ and t are the dimensionless velocity and time scaled relative to the perfect gas acoustic scale: $t = t'c'_0/L'$ and $V = V'/c'_0$ where $c'_0 = (\gamma R' T'_c)^{1/2}$ represents the sonic velocity in an ideal gas and γ is the corresponding ratio of specific heats.

The small parameter ε is defined by $\varepsilon = Prt'_a/t'_d$ (here, $\varepsilon = 2.6 \times 10^{-8}$) where Pr is the ideal gas Prandtl number (here, $Pr = \nu'_0/\kappa'_0 \approx 2.27$), ν'_0 and κ'_0 represent the kinematic viscosity and thermal diffusivity, respectively, with $t'_a = L'/c'_0$ and $t'_d = L'^2/\kappa'_0$. It should be noted that t'_d is not the characteristic time for diffusion in a supercritical fluid. Indeed, if we take into account the vanishing thermal diffusivity of near-critical fluids, this characteristic time would be of order $t'_d/\mu^{1/2}$ which is even larger (Zappoli 1992).

The dimensionless equations for continuity, momentum, energy and state are then written:

$$\frac{\partial \rho}{\partial \tau} + \nabla \cdot (\rho \boldsymbol{V}_\tau) = 0,$$

$$\frac{\partial (\rho \boldsymbol{V}_\tau)}{\partial \tau} + \nabla \cdot (\rho \boldsymbol{V}_\tau \boldsymbol{V}_\tau) = -\frac{1}{\gamma c_\tau^2} \nabla P + \frac{\varepsilon}{c_\tau} [\nabla^2 \boldsymbol{V}_\tau + \tfrac{1}{3} \nabla (\nabla \cdot \boldsymbol{V}_\tau)] + \frac{1}{Frc_\tau^2} \rho \boldsymbol{g},$$

$$\frac{\partial (\rho T)}{\partial \tau} + \nabla \cdot (\rho \boldsymbol{V}_\tau T) = -(\gamma - 1)(P + a\rho^2)(\nabla \cdot \boldsymbol{V}_\tau) + \frac{\varepsilon \gamma}{Prc_\tau} \nabla \cdot [\{1 + \Lambda (T - 1)^{-0.5}\} \nabla T] + \varepsilon \gamma (\gamma - 1) c_\tau \phi,$$

$$P = \frac{\rho T}{1 - b\rho} - a\rho^2,$$

where $Fr = c_0'^2/L'g'_0$ (here, $Fr = 8.19 \times 10^5$) is the acoustic Froude number with $g'_0 = 9.8\,\mathrm{m\,s^{-2}}$ representing the earth gravity and $\phi = (\boldsymbol{V}_\tau)_{i,j}(\boldsymbol{V}_\tau)_{j,i} + (\boldsymbol{V}_\tau)_{i,j}(\boldsymbol{V}_\tau)_{i,j} - \frac{2}{3}(\boldsymbol{V}_\tau)_{i,i}(\boldsymbol{V}_\tau)_{j,j}$ is the heat dissipation. Here, $a = \frac{9}{8}$ and $b = \frac{1}{3}$ correspond to the dimensionless coefficients of a' and b' which are calculated from the van der Waals' equation, i.e. $T'_c = 8a'/27b'$, $\rho'_c = 1/3b'$, $P'_c = a'/27b'^2$.

The no-slip boundary conditions at the cavity walls and the temperature or insulating conditions are given in figure 1.

3. Criteria for the onset of convection

The problem, which is addressed here, is the stability of a horizontal supercritical fluid layer, infinite in lateral extent, heated from below in the presence of gravity. According to Rayleigh, above a critical temperature difference, the quiescent system becomes unstable and a cellular flow develops. If the variation of density with pressure is negligible compared to that with temperature, i.e. $(\partial \rho'/\partial P')_{T'} \Delta P' < -(\partial \rho'/\partial T')_{P'} \Delta T'$, the onset of convection is determined by the Rayleigh criterion which for the incompressible case is:

$$Ra = \frac{\rho' C'_p g'}{\lambda' \nu'} \left(\frac{\partial \rho'}{\partial T'} \right)_{P'} L'^3 (T'_L - T'_U) \geqslant Ra_c, \tag{1}$$

where T'_L and T'_U are the temperature of the lower and upper walls, respectively, C'_P and λ' are the specific heat at constant pressure and the thermal conductivity. Ra_c is the critical Rayleigh number for the onset of convection and is equal to 657.5, 1707.8

and 1100.6, respectively, depending on whether the upper and bottom boundaries are both stress-free, both solid and isothermal boundaries, or one is solid and the other a free boundary (Chandrasekar 1961).

Another limiting case is also relevant and it can occur when the viscosity and thermal conductivity are neglected, but when the compressibility is taken into account; in this case, the stability criterion is that due to Schwarzchild (Landau & Lifschitz 1959):

$$\frac{\partial T'}{\partial y'} > -\frac{g'\rho'}{\beta'}(\chi'_T - \chi'_S) = -\frac{g'T'\beta'}{C'_p}, \tag{2}$$

where χ'_T and χ'_S are, respectively, the isothermal and isentropic compressibilities and β' is the thermal expansion coefficient. The term on the right-hand side of (2) represents the gradient obtained by moving a fluid particle along the hydrostatic pressure gradient (Spiegel 1965). The notion is in common use in the atmospheric sciences. The formula for gases was originally suggested by Jeffreys in 1930 and for critical fluids by Gitterman & Steinberg (1970*a*,*b*) using the hydrodynamic equations with a mean-field equation of state, similar to that used in this paper. The definition of the local Rayleigh number which accounts for these two effects in compressible flows is (Spiegel 1965; Gitterman & Steinberg 1970*b*):

$$Ra = \frac{g'L'^4\beta'\rho'C_p[((T'_L - T'_U)/L) - (g'T'\beta'/C'_p)]}{\lambda'\nu'}. \tag{3}$$

It is noteworthy that the second term of this expression (that is, the Schwarzchild term) is constant as we approach the critical point because β' and C'_p diverge with the same critical exponent. The local temperature T' ($T'_U < T' < T'_L$) is taken at its initial value which corresponds to the reference temperature T'_i. The coefficients β and χ'_T correspond to spatially independent properties because low heating cases are considered; this is consistent with the assumption of a linear regime during the early stage of the simulation where these quantities are determined.

Gitterman & Steinberg (1970*b*) have developed a model based on asymptotic analyses applicable to the onset of convection in compressible and dissipative fluids and which is here extended to near-critical fluid conditions. They determined an approximation to the critical Rayleigh number which has the following form:

$$Ra_c = \gamma_0 \frac{1 + (L'/L'_1)^4 + (L'/L'_1)^2(L'_2/L'_1)^2}{1 + (L'_3/L'_1)^4(L'_2/L')^2}, \tag{4}$$

where L' is the lengthscale of the cavity and $L'_{i=1,2,3}$ are characteristic lengths explicitly derived from Gitterman & Steinberg's pioneering works as:

$$L'_1 = \left[\frac{\gamma_0 \nu'\kappa'}{g'^2(\partial\rho'/\partial P')_{T'}(1 - C'_v/C'_p)}\right]^{1/4},$$

$$L'_2 = \left[\frac{\gamma_1 \nu'\kappa'}{(1 - C'_v/C'_p)}\left(\frac{\partial\rho'}{\partial P'}\right)_{T'}\right]^{1/2},$$

$$L'_3 = \left[\frac{\gamma_0 \nu'\kappa'}{g'^2(\partial\rho'/\partial P')_{T'}}\right]^{1/4}.$$

The magnitudes of γ_0 and γ_1 depend on the conditions at the boundaries of the fluid layer. For two solid walls, γ_0 is the incompressible critical Rayleigh number ($\gamma_0 = 1707.8$). The value of γ_1 is approximated from the case with both solid surfaces

($\gamma_1 = 70.5$). Following Zhong & Meyer (1995), we consider that the value also holds for the solid-free configuration.

From Gitterman & Steinberg's analysis, the onset of Rayleigh–Bénard instability in a near-critical fluid layer is characterized by the local Rayleigh number, derived from equation (1), which has to be compared to the critical Rayleigh number derived from equation (4). Nevertheless, Carlès & Ugurtas (1999) have discussed the approximations in Gitterman & Steinberg's model and have concluded that their developments led to heuristic criteria, but with equations which are not strictly correct. However, for the present case, both these teams' results differ by less than 0.1% over a relatively large region near the critical point. Moreover, it appears that Gitterman & Steinberg's model is more complex than required (see equation (4)) and that the results of the asymptotic analyses show that classical criteria (as taken from Spiegel 1965) can be used to estimate the threshold of convection in near-critical fluids. If the Rayleigh number defined by equation (3) exceeds the critical Rayleigh number derived for a Boussinesq fluid, then instability arises and otherwise the initial quiescent fluid layer remains stable.

Different stable and unstable regimes are predicted, depending on the proximity to the critical point and on the height of the cell. Without any lateral confinement and at a distance from T_c' (in particular at 1 K and higher), the onset of the convection regime is governed only by the classical Rayleigh number. However, near the critical point, the onset occurs later in terms of dimensional $\delta T'$ and the transition is then governed by the Schwarzchild criterion. From equation (3), the critical temperature gradient at which convection arises is:

$$(\delta T')_{onset} = Ra_c \frac{\lambda' \nu'}{g' L'^3 \beta' \rho' C_p'} + \frac{g' T' \beta' L'}{C_p'}. \tag{5}$$

The second term on the right-hand side (corresponding to the adiabatic gradient) shows small variations regardless of the proximity to the critical point. The first term becomes asymptotically small close to the critical point, whereas it is dominant far from it. Thus, as concluded by Gitterman & Steinberg (1970*b*) and by Carlès & Ugurtas (1999), if a supercritical fluid at critical density is confined between two infinite plates and subjected to an adverse temperature gradient, its convective stability will be characterized by Rayleigh's criterion far from the critical point and by Schwarzchild's criterion close to the critical point. For a comprehensive overview of all the pioneering works, refer to the paper by Gitterman (1978).

4. Stability in terms of existing analyses

4.1. *Topology of the cavity and basic phenomena*

We simulate numerically the onset of convection from rest and thermodynamic equilibrium in a two-dimensional cavity model by increasing progressively the temperature T_i' of the bottom surface of $\Delta T'$ (of some mK) over about one second and from its initial value. Owing to the vanishing thermal diffusivity, a thin initial thermal boundary layer forms and is associated with a very large, localized density gradient which expands upwards very slowly at the vanishing heat diffusion speed. Owing to the piston effect, a homogeneous bulk region is established in the core of the cavity. Bulk density (ρ_{bulk}') and temperature (T_{bulk}') can be derived from the one-dimensional asymptotic analyses of Zappoli & Carlès (1995). The bulk region settles in the core up to the vicinity of the upper cold wall which is maintained at T_i'. As the bulk temperature is much higher than the initial temperature, a second thermal boundary

layer then forms. The layer which is generated corresponds to the so-called cold piston effect (see Zappoli *et al.* 1996).

The resulting configuration comprises three major flow regions that are shown in figure 1:

(i) The stratified density layer confined below by the hot rigid wall. Its upper edge corresponds to a free, isothermal ($T' \approx T'_{bulk}$) and iso-density ($\rho' \approx \rho'_{bulk}$) boundary through which the layer merges with the bulk; its thickness h' grows at the thermal diffusion speed; the layer is open on the bulk at its upper boundary and corresponds to free conditions that are only governed by continuity; the corresponding temperature difference is denoted $\delta T'_L = T'_i - T'_{bulk} + \Delta T'$. The variable h' is a reference height of the temperature (or density) boundary layer at the bottom wall and it is determined as the distance to the wall where the local temperature (or density) reaches the bulk temperature (or density) within an estimate of about 1% of the variation: so $(T' - T'_{bulk})/(T'_L - T'_{bulk}) \approx 0.99$. The height h' is determined subsequently from the numerical data and at each timestep. Typical computed profiles for the density are shown in figure 4 for $\Delta T' = 0.1\,\mathrm{mK}$ (before the threshold) and they show that the boundary-layer profile then sharply matches at the border the value in the core. This makes it obvious that the relevant magnitudes of h' can be computed from these profiles.

(ii) The bulk region corresponding to a homogeneous density and temperature fields.

(iii) The upper layer bounded above by the upper, rigid wall and below by the homogeneous bulk region. The characteristic local temperature difference is denoted by $\delta T'_U = T'_{bulk} - T'_0$.

4.2. *The context of the existing stability theories*

The only model available among the analytical stability analyses for unconfined layers considers a lower, rigid wall with a stress-free upper boundary. We will thus assume that the difference of dynamic boundary conditions between the analytical model and the actual layer is limited and should not strongly affect the location of the threshold. The stability criterion exhibits two strong and opposite variations of $\delta T'_{onset}$ as a function of the vertical height h' of the layer. Far from T'_c, the Rayleigh criterion gives a $(1/h'^3)$-dependence while the Schwarzchild limit close to T'_c reveals a linear h'-dependence (see figure 3).

The stability of the upper layer – confined on top by a rigid cold wall and in contact with the bulk, below – has not yet been performed analytically, i.e. no result from a model involving an upper rigid wall and a stress-free boundary below is available. The upper layer proves, in fact, to be slightly more stable than the lower one. Several solutions can be postulated: both layers are stable; the lower layer is unstable and the upper one is stable; the upper one can be destabilized by the rising vortices issued from the lower layer after crossing the bulk region; and also when both layers are unstable. In the present work, some of these situations are discussed with respect to the stability analysis which focuses mainly on the threshold.

Figures 2 and 3 display the results of linear stability analyses of Gitterman & Steinberg (1970*b*) and Carlès & Ugurtas (1999). The results illustrate clearly that the variation of the critical $\delta T'_{onset}$ for fluids close to the critical point and with respect to the height h' of the density layer, is significant. Figure 2 shows the gradual transition from the adiabatic gradient condition, i.e. the Schwarzchild criterion, for inviscid, compressible fluids, near the critical point, to the Rayleigh condition corresponding to the onset of viscous convection flow far from the critical point. The stability limits

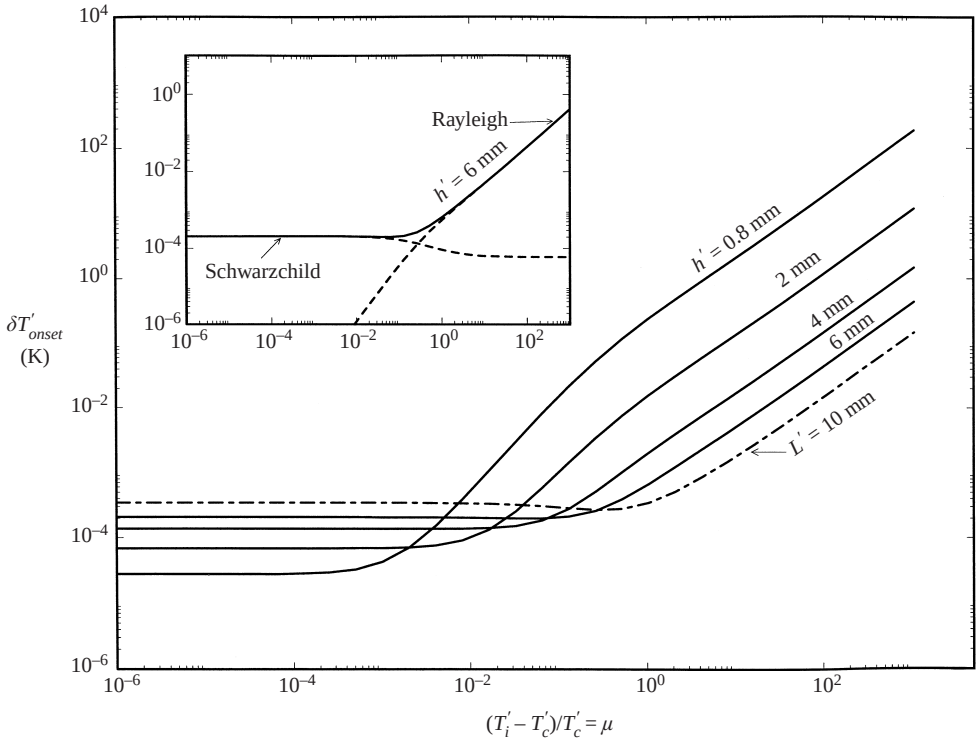

FIGURE 2. Critical $\delta T'_{onset}$ (K) at the onset of convection as derived from Rayleigh and Schwarzchild criteria, Equation (5), versus μ, the distance to the critical temperature T'_c. The characteristic lengthscales are the local height of the hot layer h', $0 < h' < L'$, and also at the limit the total height of the cavity L'. The respective contributions of the Rayleigh and Schwarzchild criteria are identified and zoomed at the left top-hand side of the figure for $h' = 6$ mm.

on $\delta T'_{onset}$ are displayed in terms of μ for several values of the height h' of the layer ranging from 0.8 mm to 10 mm. These values are chosen in order to correspond to actual heights of the bottom layer during the simulations at times ranging over a few seconds after the start of heating. The values corresponding to the full height, $L' = 10$ mm, of the cavity are cited as a reference. At this value of $h' = L'$, the $\delta T'_{onset}$ curve corresponds to the stability of the layer confined by the two rigid walls. We notice from figure 2 that the values of the asymptotic $\delta T'_{onset}$ limit derived from the Schwarzchild criterion at small μ grow linearly with h' whereas the $\delta T'_{onset}$ from the Rayleigh criterion decreases as $1/h'^3$ at large values of μ. The contributions of the two criteria to the actual stability of the system are shown in the top left-hand corner of figure 2 for $h' = 6$ mm. Figure 2 exhibits a narrow zone of $0.1 < \mu < 1$ where the actual criterion can differ by about 100% from either the Rayleigh or Schwarzchild criterion if considered separately.

During the process for $T'_i - T'_c$ as large as 1 K ($\mu \approx 0.003$), the growth of the thermal layer is very slow and the magnitude of the local height h' at the onset of vortices is nearly 0.8 mm, and this remains about the same value over a large number of PE timescales. This height is the relevant h' value that corresponds to the threshold criterion. Figure 2 suggests that through the mixing process due to convection or due to the growth of the layer height h', the characteristic local $\delta T'_L$ can decrease and become smaller than $\delta T'_{onset}$ for some h'. Thus, the possibility of the damping of the convection exists.

Conditions	β (K^{-1})	χ_T (Pa^{-1})	λ ($W\,m^{-1}\,K^{-1}$)	C_p ($J\,kg^{-1}\,K^{-1}$)
Supercritical fluid	0.66	0.5×10^{-5}	0.23	5.8×10^{4}
Perfect gas	3×10^{-3}	9.8×10^{-8}	3.85×10^{-2}	660

TABLE 1. Thermo-physical properties for CO_2: supercritical fluid conditions and the perfect gas conditions.

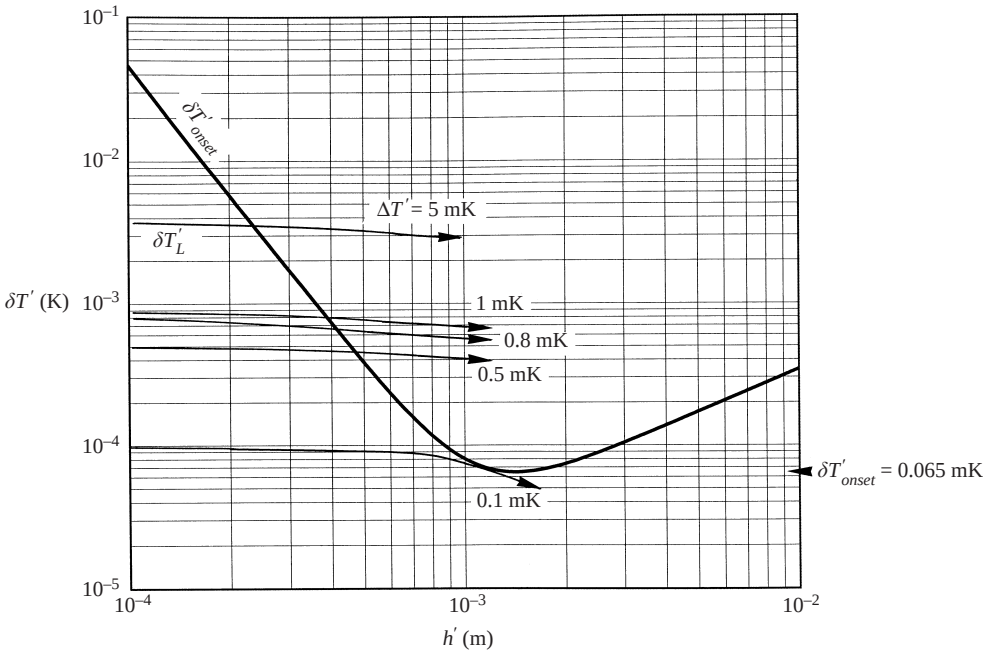

FIGURE 3. Theoretical critical, $\delta T'_{onset}$ (K), as a function of the local height, h', of the hot bottom layer as given by equation (5). The curves with arrows represent the evolution with time of the successive local $\delta T'_L$ computed between the edge of the hot bottom layer and the wall and for different values of the total temperature difference $\Delta T'$ applied between the two horizontal walls of the cavity: $\Delta T' = 0.1$, 0.5, 0.8, 1 and 5 mK. The arrows indicate the sense of the variation of $\delta T'_L$ with h', then with time. The crossing of the theoretical stability curve gives the theoretical estimate of $\delta T'_L$ and h' at the onset of instabilities in the hot layer. The minimum of theoretical $\delta T'_{onset}$ is indicated, 0.065 mK.

Figure 3, as directly derived from (5), gives the critical $\delta T'_{onset}$ as a function of h' over a range of h' which is relevant to the size of the cavity, $h' < 10$ mm. The physical coefficients in (5) were evaluated at temperature T'_i that we recall being 1 K above the critical temperature. They are reported in table 1. The curve confirms a cubic dependence, i.e. $1/h'^3$, following the Rayleigh criterion at small h', and a linear dependence in h' following the Schwarzchild criterion at larger $h' < L' = 10$ mm.

5. The numerical approach

5.1. *The numerical method*

We consider the two-dimensional square cavity with 10 mm sides filled with CO_2 on the critical isochore and initially at 1 K above its critical temperature. Table 1 gives

$(\Delta T')$ (mK)	Boundary-layer thickness h' (mm)	$(\delta T)_L$ (mK)	Ra (from (1))	Ra (from (3))	Ra_c (from (4))
10.0	0.80	5.732	70 055	69 719	1435
5.0	0.70	3.008	24 626	24 431	1296
2.5	0.60	1.285	6625	6519	1206
1.0	0.55	0.726	2883	2808	1175
0.8	0.52	0.62	2081	2021	1160
0.5	0.50	0.45	1342	1291	1151
0.1	0.35	0.09	92	80	1112
	0.50	0.09	269	217	1151
	0.75	0.09	906	646	1360
	1.0	0.09	2148	1328	1920

TABLE 2. The computed Rayleigh numbers are determined from equation (1) as derived from the incompressible case, from the local Ra relation (3) which takes the compressible flow effects into account and from (4) which is derived from Gitterman & Steinberg (1970*b*) stability analysis. The estimates of the boundary-layer thicknesses at the bottom of the cavity and of the local temperature difference at the edge of the layer are derived from the computed solutions at several given $\Delta T'$.

the corresponding physical properties as well as those for CO_2 for an ideal gas. These properties differ by several orders of magnitude.

The governing equations are solved numerically by a finite-volume method using the SIMPLER algorithm (Patankar 1980). The time discretization is of implicit Euler type and first-order accurate, and the discretization in space uses the power-law scheme (Patankar 1980). When approaching the critical point, the boundary layer becomes thinner and thinner, and a fine grid size is required in order to ensure a sufficiently small grid Péclet number. A non-uniform staggered mesh has then been used, and numerical stability has been tested carefully in terms of timestep and grid size. In order to reduce computational time, an acoustic filtering procedure has been used (Paolucci 1982) when the description of the acoustic wave is not required. Zappoli *et al.* (1996) and Amiroudine *et al.* (1997) provide more details on the numerical solver.

Mesh-independent numerical solutions are considered using graded meshes of 101×81 to 121×121 in which about 50% of the grid comprises points inside the thin layers to be studied. In particular, we concentrate about 30 points in the vertical direction within the layers, 0.5–1 mm thick, that play a dominant role in the phenomenon. The mesh size near the walls is as small as 2×10^{-4} mm in the finer mesh. The timestep is kept constant at about 1.25×10^{-3} s which corresponds to 800 timesteps to compute the heating stage of about 1 s. The accuracy of the numerical solution has been studied by Amiroudine (1995) and Amiroudine *et al.* (1997). The control of the accuracy is very important in the investigation of this time-dependent phenomenon.

5.2. *The numerical investigation*

The onset of convective vortices arising from the hot bottom layer is simulated for several linear temperature increases of the bottom wall, 10, 5, 2.5, 1, 0.8, 0.5 and 0.1 mK, over time periods of 0.1–1 s. The temperature gap is initiated over the two first grid points near the bottom wall. Here, we mainly detail the determination of the threshold value and give some insights into the flow structure. The conditions that have been investigated are given in table 2.

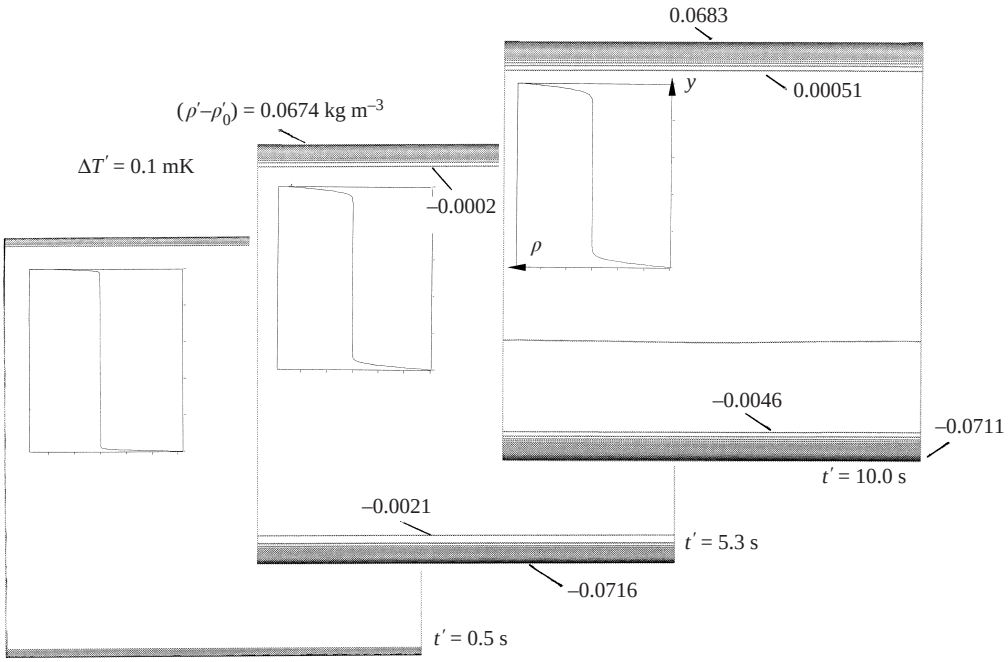

FIGURE 4. The density patterns and the respective density profiles along the vertical axis are given at several time stages during the heating process for $\Delta T' = 0.1$ mK. Stable iso-density configurations (that do not exhibit any convection effect) display the growth of the density layers at given timesteps. The density is given as the $(\rho' - \rho'_0)$ in kg m^{-3} units in the pattern displays. The values are printed in the patterns at their respective locations and at some instants: at the top and bottom walls and on two iso-density lines of interest, at the borders between the core zone and the density layers. Successive instants and $(\rho' - \rho'_0)$ values are: $t'(\rho'_{top} - \rho'_0,\ \rho'_{bottom} - \rho'_0) = 0.5$ s, 5.3 s (0.0674 kg m^{-3}, -0.0716 kg m^{-3}) and 10 s (0.0683 kg m^{-3}, -0.0711 kg m^{-3}).

In order to interpret our results within the framework of existing theories, we measure from the output files, when the instability starts, the parameters such as the height h' of the layer and the temperature drop $\delta T'_L$ that must be considered in the analogy with the ideal situations quoted earlier. The time at which the instability is triggered is determined by noting when the isotherms become disturbed by the flow field, in other words, when the deformations that first appear in the two bottom corners show the effect of vertical convective transport. The height of the layer to be considered to interpret the numerical results is taken as the average value between the height where the extension of the linear temperature drop reaches the bulk temperature and the height of the bulk isotherm. This is a good approximation since the matching between the boundary-layer temperature drop and the bulk is of very small spatial extent (see density profiles in figure 4). The measurement of the lengths themselves are given by the numerical code without any further errors other than that coming from the numerical method and the model. It should also be noted that accounting for the thermo-acoustic effect is essential to estimate the actual temperature drop in the layer since the bulk temperature changes with time.

The use of the stability criterion for layers that are subjected to a steady gradient implies the assumption that the slowest growing mode still grows at a faster rate than the diffusion timescale that governs the expansion of the unperturbed pure diffusion layer. The better this criterion is, the smaller is the heat diffusivity, which is indeed

the case for a near-critical fluid. It would be possible to check this hypothesis *a posteriori* by measuring the growth exponent as a function of the wavenumber of the perturbations. However, the outputs of the numerical simulation confirm that the instability grows much faster than the growth of the thermal boundary layer. In fact, the thermal boundary-layer thickness, h', evolves as $\sqrt{t'}$ in time via a thermal diffusion process. The relative timewise amplification of the perturbation near the threshold, as given by the computations at 1 K above the critical point, is approximately 0.3–0.7 s^{-1} when $\Delta T'$ is 0.5–5 mK. The relative expansion in the thermal layer thickness, $h'^{-1}\mathrm{d}h'/\mathrm{d}t'$, decreases as $1/t'$ in s^{-1}. We consider that the thermal layer height is nearly frozen just before the onset of convection when the comparison is made with the stability analyses.

6. Results and discussion

6.1. *The threshold at the hot bottom layer*

The evolution of the local temperature difference between the bottom wall and the edge of the thermal boundary layer, $\delta T'_L = T'_i + \Delta T' - T'_{bulk}$, is represented in figure 3 for several $\Delta T'$. We note that the evolution of the gradient remains regular over a certain period of time because the shape of the layer remains unaffected immediately after the threshold of convection. The curves $f(\delta T'_L, h')$ in figure 3 represent the evolution in time of the hot layer in the cavity and they obviously cross the stability curve corresponding to a Rayleigh instability for several $\Delta T'$. The arrows indicate the direction of elapsed time. For $\Delta T' = 0.1$ mK, no convection is observed in the simulation and the corresponding curve in figure 3 is below the stability extremum near the changeover point between the Rayleigh and Schwarzchild instability modes.

We notice from figure 3 that for small h', i.e. close to the beginning of the heating (consider $h' = 0.1$ mm as reference), the theoretical critical local $\delta T'_{onset}$ corresponding to the temperature drop in the layer (see the thick curve in the figure which starts at $\delta T'_{onset} \approx 45$ mK for $h' = 0.1$ mm), is larger than the total temperature differences $\Delta T'$ itself (for the present we have imposed $0.1\,\mathrm{mK} < \Delta T' < 10\,\mathrm{mK}$ at the bottom wall with respect to the upper wall at T'_i). In figure 3, the curve corresponding to the variation of the temperature drops in the lower layer, $\delta T'_L$, for $\Delta T' = 5$, 1, 0.8, 0.5 mK crosses the stability curve, $\delta T'_{onset}$, at $h' \approx 0.25$ mm then over a range of h' roughly between 0.4 and 0.5 mm. We note that this first threshold is determined by Ra_c. Thus, the first stages of the heating process would be expected to be stable before these values of h' are reached at the onset of convection, at Ra_c. Then, the configuration should become unstable at about $h' = 0.4$ mm when $\Delta T' \approx 1$ mK. The layer can grow at the thermal diffusion velocity rate, but it will then remain unstable as long as the local temperature difference $\delta T'_L = T'_i + \Delta T' - T'_{bulk}$ remains larger than approximately 0.065 mK, which is the minimum of the stability curve $\delta T'_{onset}$ at a height of about 1.5 mm. Moreover, we note in the second part of the curve (right-hand side with respect to this height) that there is a second change of stability, the relevant threshold of which is determined by the Schwarzchild criterion, when $h' > 1.5$ mm and $\delta T'_L > \delta T'_{onset} > 0.065$ mK. It is seen that in the case of the 10 mm high cavity with $\Delta T'$ of 1 mK, the process should remain unstable throughout. Since the local $\delta T'$ in the hot and cold layers consists of two parts, it is possible when the $\Delta T'$ between the walls is less than about 0.5 mK, that the local $\delta T'_L$ falls below the Schwarzchild limit during the process, which would then determine a reverse transition back to a stable configuration.

The local critical Rayleigh number is deduced from measurements of the height h'. In the calculation of the critical Rayleigh number we have used the hot wall condition at the solid bottom boundary and the temperature at the free top isothermal surface that limits the layer that is known from the simulation. The characteristic length h' is defined by the height of the thermal layer whereas the magnitude of the temperature gradient is derived from the linear part of the profile. Table 2 gives the values of the different physical parameters obtained from the numerical solution, i.e. the thickness of the thermal boundary, the local temperature gradient and the corresponding local and critical Rayleigh numbers derived from equations (1), (3) (including the Schwarzchild correction) and (4), respectively.

In the present unsteady configuration, the Rayleigh number increases because of the heating process. Consequently, if at the beginning of the heating, the flow configuration is unstable, it may remain unstable or become stable at subsequent times (see figure 3) even if the boundary-layer thickness increases during the slow diffusive process. Nevertheless, in the case where the configuration is stable at the beginning, it could become unstable later because the Rayleigh number increases continuously up to the end of the diffusion process.

The height, h', evolves with time, as $\alpha t^{1/2}$, α depending on the physical fluid properties at T_i' and more weakly on the temperature step $\Delta T'$. Its variation has been checked over the first 1–20 s of simulation, which corresponds to a period where no disturbance has arisen. In the case of $\Delta T' = 0.1$ mK, there is no onset and the behaviour covers the entire simulation. At larger $\Delta T'$ the growth is broken by the rise of plumes inside the layer. We note that an estimate of the speed of the growth of the thermal layer is nearly $0.03\,\mathrm{mm\,s^{-1}}$.

As shown in figure 3, the stability for layers of small height at 1K from the critical point (which is relatively far away) is determined mainly by the Rayleigh criterion. This is confirmed in table 2 since nearly the same values of the Rayleigh number are obtained from equations (1) and (3) which means that the Schwarzchild term is negligible. The critical Rayleigh number has been obtained from equation (4) with solid-free boundary conditions. In most cases, the comparison confirms the simulation of an unstable numerical solution because the local Ra is above Ra_c. This is the case for $\Delta T'$ down to 0.5 mK where $Ra = 1291$ is the closest to $Ra_c = 1151$. At $\Delta T' = 0.1$ mK no convection was predicted; we evaluated the stability conditions for increasing h'. The critical Ra_c was always above the local Ra and, moreover, the contribution of the Schwarzchild criterion near $h' = 1$ mm started to be dominant. We note that this contribution significantly decreases the local Ra that would be larger than Ra_c if only the Rayleigh criterion was used, equation (1).

The computed local Rayleigh number derived from equation (3) and the critical Ra_c from equation (4) confirm the analysis of table 2 as local Ra are above the critical Ra_c curve for all the cases except for the case $\Delta T' = 0.1$ mK with h' considered up to 1 mm. The time elapsed from the start of heating until the convection arises and significantly disturbs the stratified density and temperature profiles in the hot layer (as seen in figure 4 *et seq.*) has been considered for the different values of $\Delta T'$. We note that the elapsed time decreases rapidly with increasing $\Delta T'$ and tends toward an asymptotic limit of about 5 s when $\Delta T'$ is larger than 4 mK. We have estimated the growth rate of the convection immediately after its onset using a linear approximation. At a given point, we note that the rate, $(v'^{-1}\mathrm{d}v'/\mathrm{d}t')$, varies from $0.3\,\mathrm{s^{-1}}$ at 0.5 mK to about $0.7\,\mathrm{s^{-1}}$ at 5 mK, which suggests a variation of approximately $(\Delta T')^{1/2}$. We have also studied the wavelength of the instability in all the situations considered, and have found an aspect ratio with respect to the height h' of the thermal layer of about 1.6.

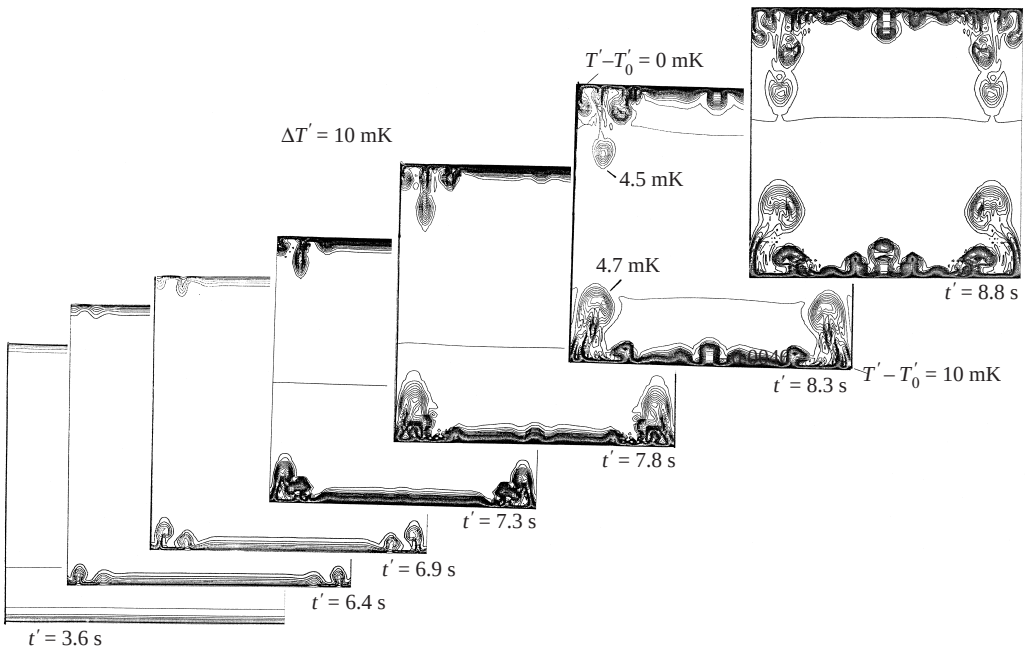

FIGURE 5. Temperature patterns at several time stages after the heating of the bottom wall for $\Delta T' = 10$ mK. Timesteps are: $t' = 3.6$ s, 6.4 s, 6.9 s, 7.3 s, 7.8 s, 8.3 s and 8.8 s. Some isotherm values, defined as $(T' - T'_0)$ in mK, are given at $t' = 8.3$ s. The patterns display the onset of 9 thermal plumes after the threshold of convection.

This is nearly independent of $\Delta T'$ in the range 0.5–10 mK. Another measure of the scale of the instability is the period of time which separates the rise of two successive thermal plumes in the numerical solution. The timescale reduces from 7 to 2 s as $\Delta T'$ increases from 2.5 to 5 mK and it becomes much larger at about 9–11 s as we become closer to the threshold for 0.8 and 0.5 mK. The proximity to the lower $\Delta T'$ that produces the onset of convection plumes is assessed by the two following features when considering the properties of the convection process at neighbouring $\Delta T' = 1$, 0.8 and 0.5 mK: (i) the elapsed time at the onset of convection steeply increases when diminishing $\Delta T'$; (ii) the timescale between two successive plumes becomes much larger when $\Delta T'$ becomes closer to 0.5 mK. From this behaviour, we estimate the proximity to the threshold to be bounded by 0.1 and 0.5 mK. Additional secondary oscillations of shorter periods subsequently appear after the onset of the preliminary oscillations at these two $\Delta T'$. The variation with $\Delta T'$ of the frequency is nearly linear in this range.

6.2. *Flow-field description*

Flow, density and temperature patterns are displayed during significant stages of the convection process in figures 4 to 8. The growth of both hot and cold thermal layers remains unperturbed by the convection when $\Delta T' = 0.1$ mK. Significant density patterns are shown in figure 4 at several times over about 10 s of the initial heating period. The vertical density profiles show the temporal variation of the density gradients near the horizontal walls. The height of the hot layer grows by a factor of four during the process. The history of $\delta T'$ versus $h'(t')$ is displayed for various $\Delta T'$ in figure 3. It is noteworthy that for this case, i.e. $\Delta T' = 0.1$ mK, $\delta T'$ remains just

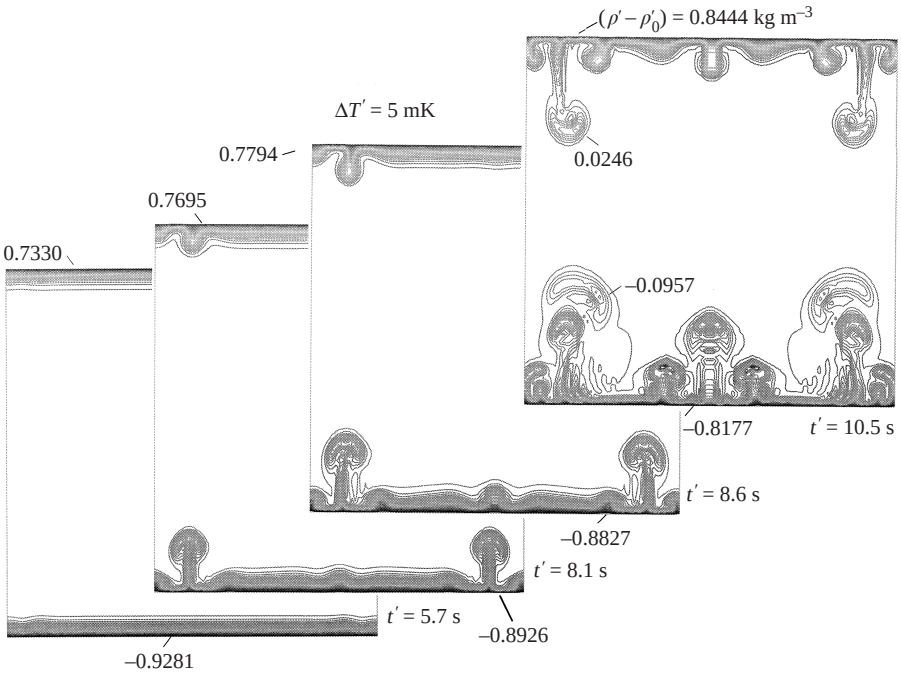

FIGURE 6. Density patterns at several stages after the heating of the bottom wall for $\Delta T' = 5$ mK. Several iso-density values, given as $(\rho' - \rho'_0)$ in kg m^{-3} units, are given at the walls and around the plumes. Timesteps and respective $(\rho' - \rho'_0)$ given at the top and bottom walls are: $t'(\rho'_{top} - \rho'_0, \rho'_{bottom} - \rho'_0) = 5.7$ s (0.7330 kg m^{-3}, -0.9281 kg m^{-3}), 8.1 s (0.7695 kg m^{-3}, -0.8926 kg m^{-3}), 8.6 s (0.7794 kg m^{-3}, -0.8827 kg m^{-3}) and 10.5 s (0.8444 kg m^{-3}, -0.8177 kg m^{-3}). The patterns display the onset of 7 thermal plumes after the threshold of convection.

below the stability limit. The (h') histories for the other computed cases, $\Delta T' = 0.5$, 0.8, 1 and 5 mK, cross the stability curve and this is consistent with the fact that they generate instabilities.

When $\delta T'_L$ is sufficiently high and the height h' exceeds the threshold value, convection can start slowly and increase progressively inside the hot layer. During a time which can be of a few seconds, convection remains weak and does not affect the density and temperature isocontours. The larger the magnitude of $\Delta T'$, the smaller is the magnitude of the critical height h'. Then, since the aspect ratio of the instability is scaled (with respect to h') to be constant and nearly 1.6 (as introduced earlier), the instability is smaller at large $\Delta T'$ than at small $\Delta T'$. This suggests that the rate of convection is also smaller near the onset. We notice that at $\Delta T' > 2.5$ mK, there is a balance between the magnitude of convection and the height h', since the time of the onset of disturbances at the edge of the hot layer is nearly constant and remains at about 5 s. Later, after the onset, the motion moves into the whole cavity and exhibits strong convective structures at large $\Delta T'$. We may also point out that, owing to the larger critical h' at larger $\Delta T'$, the layer generates for the same width L' a larger number of disturbances than it does for smaller $\Delta T'$. This has a great impact on the thermal homogenization of the cell.

Convection inside the cavity can be inferred from the temperature (and density) patterns. There is an upward and downward movement of hot plumes of gas from the hot layer below and of cold ones from the cold layer above into the bulk in the

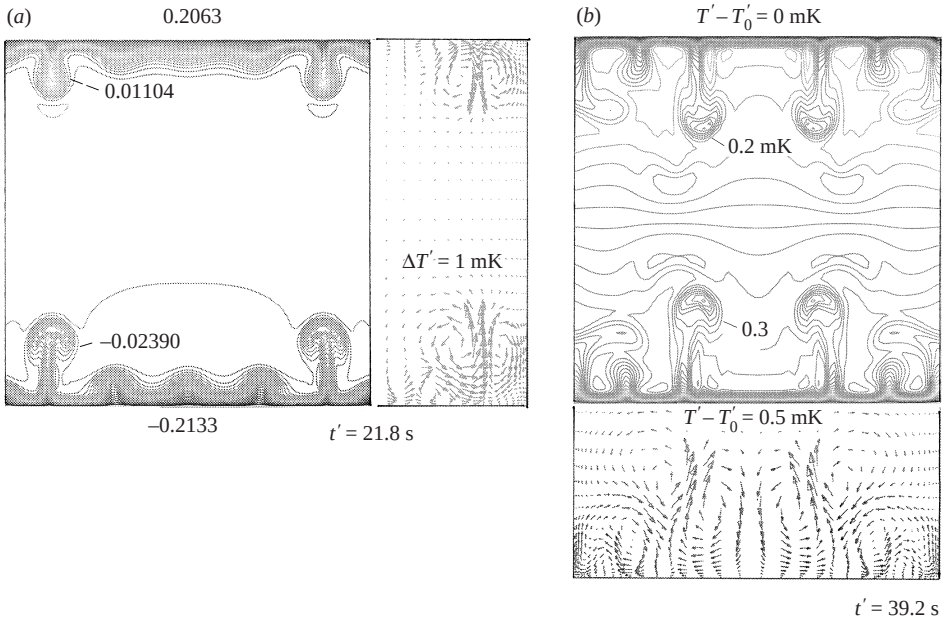

FIGURE 7. Density and temperature patterns together with the velocity fields – represented near one side-wall and in the bottom layer – for $\Delta T' = 1\,\mathrm{mK}$ and $0.5\,\mathrm{mK}$ at two timesteps after the threshold of convection. (*a*) At $\Delta T' = 1\,\mathrm{mK}$, the patterns display the onset of 5 thermal plumes. Density values are printed as $(\rho' - \rho'_0)$ in $\mathrm{kg\,m^{-3}}$. The magnitude of the velocity, $|V_{max}|$, is given in $\mathrm{mm\,s^{-1}}$: $t'(|V_{max}|) = 21.8\,\mathrm{s}$ $(0.94\,\mathrm{mm\,s^{-1}})$. Associated local Reynolds numbers, $Re = |V_{max}|h'/\nu'_0$, is about $Re \approx 12.8$. Respective $(\rho'_{top} - \rho'_0, \rho'_{bottom} - \rho'_0)$ are $(0.2063\,\mathrm{kg\,m^{-3}}, -0.2133\,\mathrm{kg\,m^{-3}})$. (*b*) At $\Delta T' = 0.5\,\mathrm{mK}$, the patterns display the onset of 6 thermal plumes. The maximal velocity magnitudes, $|V_{max}|$ in $\mathrm{mm\,s^{-1}}$, on the mesh points, and the corresponding local Re are: $t' = 39.2\,\mathrm{s}$ $(0.61\,\mathrm{mm\,s^{-1}}$, $Re \approx 8.3)$. Characteristic temperature values, defined as $(T' - T'_0)$ in mK, are given in the figure at the walls and at the edges of the two boundary layers.

middle of the cavity. Convection cells also transport cold eddies of gas to the heated wall that constrain the thermal layer by restricting its height. This can be observed by comparing temperature patterns before and after the initiation of convection in figures 5 to 8. The velocity fields exhibit a vortex motion evident in figures 7 and 8, for $\Delta T' = 1\,\mathrm{mK}$, $0.8\,\mathrm{mK}$ and $0.5\,\mathrm{mK}$. The first case has five structures of instability, the other two have six. These structures that develop along the edge of the thermal boundary layer result from the motion originating near the lateral insulated walls. The disturbances generate a similar number of cells in the cold layer, but thus is relatively weak and delayed. Successive cells grow progressively and fill the entire layer. They grow in magnitude and in size and move upward in the bulk region. The local Reynolds number is estimated as $Re = |V_{max}|h'/\nu'_0$ from the maximum velocity in the vortices, $|V_{max}|$, and from the boundary-layer thickness, h', as the lengthscale. Their values remain small and range from about 1 to 13 for the three configurations and during the considered time of the process. Figures 7 and 8 cover about 20–40 s of the scenario of the growth until plumes of hot gas break away from the hot layer and migrate up into the bulk. Secondary vortices are shown to arise below the primary corner vortices for 1 mK. We notice on that time period that there is no real bulk interaction between the vortices originating from either layer.

We may notice in the temperature and density patterns for 10 and 5 mK (figures 5 and 6) that the vortices grow and expand more quickly at larger $\Delta T'$. The vortex-

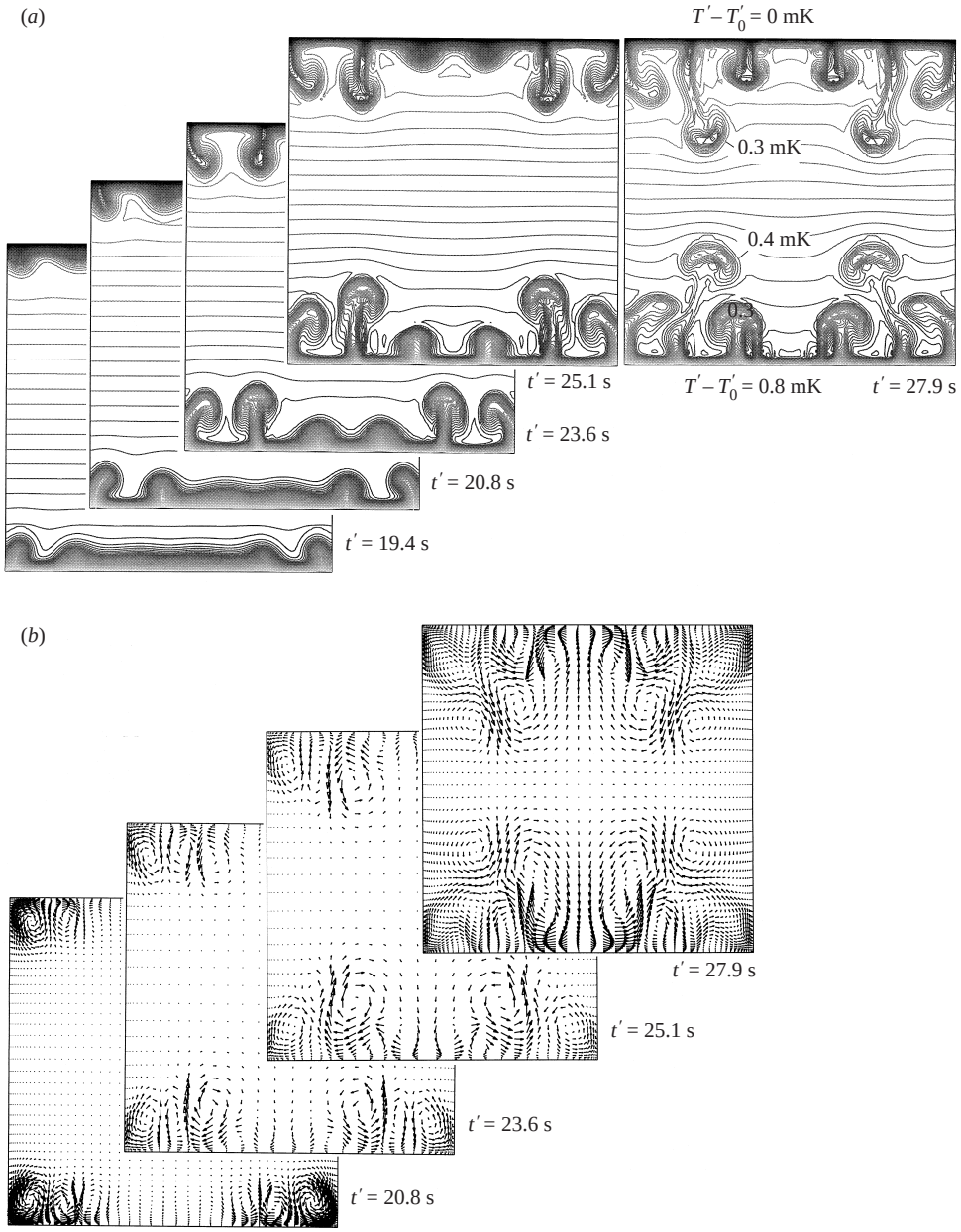

FIGURE 8. Temperature patterns (*a*) and relevant velocity fields (*b*) for $\Delta T' = 0.8$ mK at several time stages after the heating of the bottom wall. Timesteps are $t' = 19.4$ s, 20.8 s, 23.6 s, 25.1 s and 27.9 s. The patterns display the onset of 6 thermal plumes after the threshold of convection. Characteristic temperature values, defined as $(T'-T'_0)$ in mK, are given with the isotherm pattern at time $t' = 27.9$ s (*a*). The maximal velocity magnitudes, $|V_{max}|$ in mm s^{-1}, and corresponding local *Re* are computed on the mesh points for the velocity fields (*b*) at the successive $t' = 20.8$ s (0.37 mm s^{-1}, $Re \approx 5$), 23.6 s (0.85 mm s^{-1}, $Re \approx 11.5$), 25.1 s (0.78 mm s^{-1}, $Re \approx 10.6$), 27.9 s (0.70 mm s^{-1}, $Re \approx 9.5$).

generating layers are much thinner and the 10 and 5 mK runs exhibit respectively 9 and 7 cells for elapsed times as small as 9 s and 10.5 s. (We may recall that 25–40 s are needed to generate 5 to 6 cells for $\Delta T' \leqslant 1$ mK).

For about 10 s the two families of hot and cold vortices still remain within their

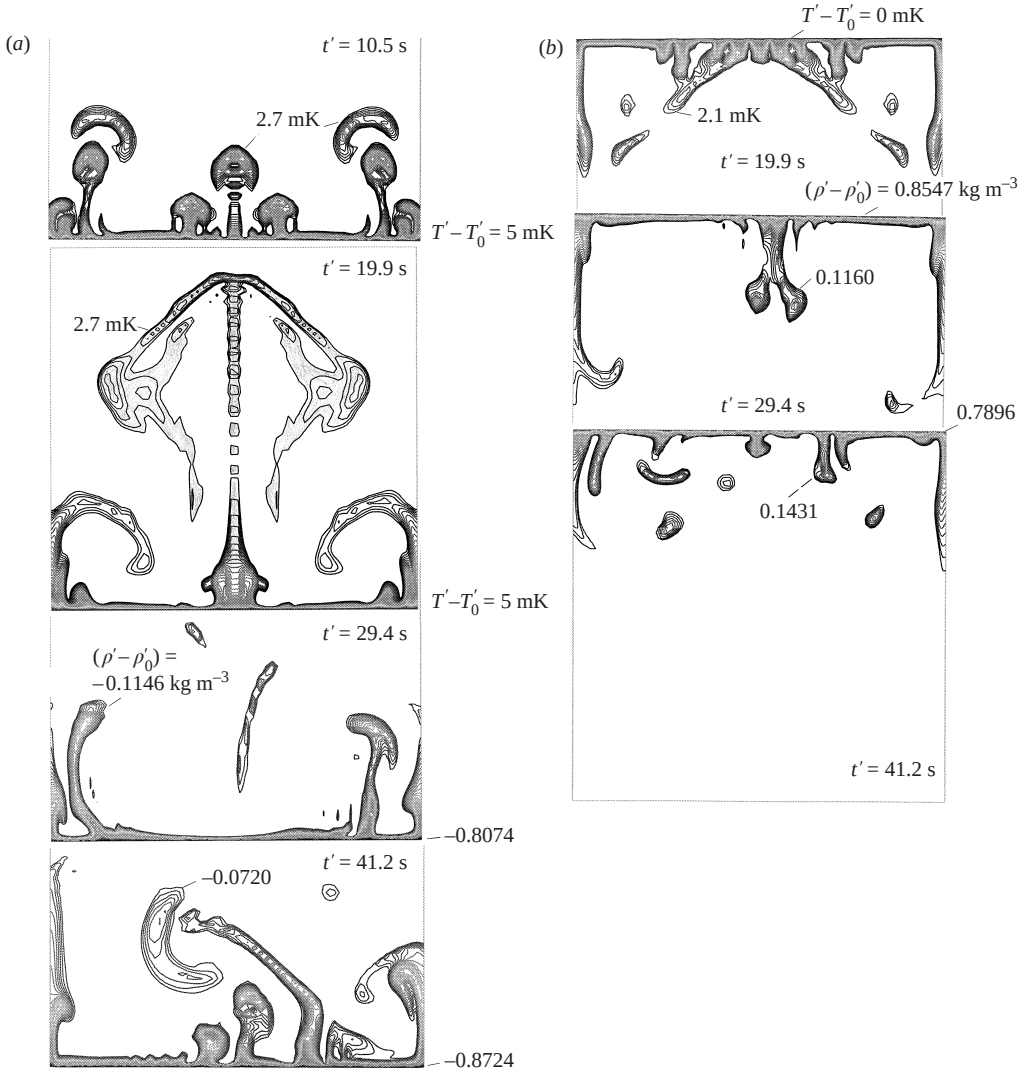

FIGURE 9. Typical temperature and density patterns for $\Delta T' = 5\,\mathrm{mK}$ at several time stages: $t' = 10.5\,\mathrm{s}$, $19.9\,\mathrm{s}$, $29.4\,\mathrm{s}$ and $41.2\,\mathrm{s}$. (*a*) Plume structures initially arising from the hot layer below at $t' = 10.5\,\mathrm{s}$; large-scale structures expanding up close to the top wall of the cavity at $t' = 19.9\,\mathrm{s}$; asymmetric small-scale structures arising after the break of symmetry near the bottom at $t' = 29.4\,\mathrm{s}$ and $t' = 41.2\,\mathrm{s}$. (*b*) Associated structures resulting from the interaction of the ascending plumes with the cold layer above. The iso-values, that are displayed, correspond to a large range of the variation of the variables – of about 40% – inside the cavity. They are concentrated with respect to the closest local extrema near (*a*) the lower and (*b*) the upper walls. Characteristic values of the temperature, defined as $(T' - T'_0)$ in mK, and of the density heterogeneities, defined as $(\rho' - \rho'_0)$ in $\mathrm{kg\,m^{-3}}$, are given around the plumes and the structures.

respective half cavities. We have tracked particular convective structures in the case $\Delta T' = 5\,\mathrm{mK}$ by simulating the motion for up to 45 s (175 timescales). The size of the vortices grows rapidly up to 60 to 70% of the cavity height. Some of the structures cross the bulk and reach the upper layer that is much less active than the lower one. These structures are apparent in figure 9 by displaying the density and temperature isocontours (which are close to each other) from the bottom to within about 45%

of their total variation. We note: (i) first the small plumes arise from the hot layer and move upward at about $t' = 10.5$ s; (ii) then the central large structure enlarges and reaches the cold wall at $t' = 19.9$ s; (iii) after this stage, a break of symmetry occurs that precedes the impact on the upper wall at $t' = 25$ s. This is illustrated with two patterns at $t' = 29.4$ s and $t' = 41.2$ s. In figure 9(*a*) we note that the structures are then very thin and vertically elongated. They are very unstable but seem to remain confined to the lower half cavity. Figure 9(*b*) concerns the upper layer and shows the isocontours corresponding to about 42% variation of the temperature and density with respect to the cold wall. The patterns for $t' = 19.9$ s reflect the interaction of the stronger structure, see figure 9(*b*), and the two others, $t' = 29.4$ s and 41.2 s, the corresponding states following the break of symmetry. The patterns reflect similar features to those in the hot zone but are characterized by smaller structures and weaker disturbances. For 10 mK, the break of symmetry (resulting from the symmetry of the boundary conditions) occurs earlier at 12.5 s. For 0.5 mK, the vortices are still confined inside the first $\frac{1}{3}L'$ of the height after 70 s and the first vortex–vortex interaction occurs without a break of symmetry after 89 s. At 0.8 mK the initial confinement stage was also confirmed up to 56 s of simulation time.

7. Conclusion

A two-dimensional unsteady numerical simulation has been performed for the highly compressible, low-heat diffusing fluid together with a van der Waals equation of state. This has been applied to the Rayleigh–Bénard problem for near-critical fluids. Owing to the vanishing of the thermal diffusivity near the critical point, the diffusive process is very slow. The heating process at the bottom wall produces a piston effect that drives the convection inside narrow thermal layers near the horizontal walls on the low heat-diffusing timescale. The first results of this study are in agreement with the theoretical predictions of Gitterman & Steinberg (1970*a,b*) for Rayleigh numbers ranging below and above the critical value. In the asymptotic limit, we note that these authors have shown that classical criteria still hold for near-critical fluids.

We have noted that if the local Rayleigh number is above the critical value, the flow will become unstable after a long diffusive process which depends on the local temperature difference $\delta T'$. On the other hand, even if the flow field is initially stable, it can be unstable later because the diffusive length increases with time whereas the temperature difference reaches a maximum. We have shown that the Rayleigh criterion determines the first instability at 1 K from T_c' whereas the Schwarzchild criterion could determine a reverse transition to no-flow if $\delta T'$ is small enough and if the height of the layer still increases regularly after the Rayleigh convection threshold. Work is in progress on this point (Raspo *et al.* 1999) and also concerning the homogenizing process following the break of symmetry of the convection pattern (Larroudé *et al.* 1997) and the effect of the distance to the critical point (Gilly *et al.* 1999).

We have shown that the unstable hot and cold diffusive layers lead to plume-type flows. A surprising result was that the upper wall also exhibits thermal instabilities. However, this result is consistent with earlier analyses (Zappoli & Carlès 1995; Carlès 1995) which have shown that when a closed one-dimensional cell initially at an uniform temperature is heated at one end, the opposite wall exhibits a cold thermal diffusive boundary layer owing to a (cold) piston effect. This feature has also been observed experimentally (Garrabos *et al.* 1998). In our two-dimensional simulation, this diffusive layer which is heavier than the bulk fluid located below, gives birth to

'drops' by a gravitational instability reminiscent of that of Rayleigh–Taylor (Zappoli *et al.* 1997). In fact, Kurowski, Misbah & Tchourkine (1995) showed the stability of two incompressible, miscible, density mismatched fluid layers, to be dominated by a dispersion relation where diffusion plays a role analogous to surface tension in non-miscible fluids. This led them to call this instability process a 'Rayleigh–Taylor-like' instability. We recently showed that a similar situation exists in near-critical pure fluids where heat diffusion associated with the diverging compressibility plays the role of mass diffusion between miscible fluids (Zappoli *et al.* 1997). In the present situation, the growing upper layer instability mechanism that produces 'drops' is reminiscent of that kind of instability for a vanishing thickness of the upper, cooler and heavier, layer. We shall attempt to show in a forthcoming paper that near-critical fluids exhibit a continuum of situations between the Rayleigh–Taylor-like instability process and the present cooled-from-the-top Rayleigh–Bénard configuration for vanishing upper layer heights.

The authors gratefully acknowledge support from the Centre National d'Etudes Spatiales (CNES), the Centre National de la Recherche Scientifique (CNRS) and the IDRIS Computing Center (Orsay). They acknowledge Dr J. Ouazzani, Professor R. L. Sani and Professor B. E. Launder for fruitful discussions and help. P. B. acknowledges the CNES for successive support over three one-year post-doctorate grants of P. L., of S. A. and also of Dr I. Raspo who made a substantial and generous contribution to the final stages of this work.

REFERENCES

Amiroudine, S. 1995 Modélisation numérique des phénomènes de transport de chaleur et de masse dans les fluides supercritiques. PhD dissertation, Université de la Méditerranée, Marseille.

Amiroudine, S., Larroudé, P., Bontoux, P. & Zappoli, B. 1996 Numerical simulation of convective instabilities in near-critical fluids. In *Proc. Second European Symp. 'Fluids in Space', Naples, Italy, April 1996* (ed. A. Viviani), pp. 37–42. Jean Gilder Congress Publications, Naples.

Amiroudine, S., Ouazzani, J., Carlès, P. & Zappoli, B. 1997 Numerical solutions of 1-D unsteady near-critical fluid flows using finite volume methods. *Eur. J. Mech.* B *Fluids* **16**, 665–680.

Assenheimer, M. & Steinberg, V. 1993 Rayleigh–Bénard convection near the gas–liquid critical point. *Phys. Rev. Lett.* **70**, 3888–3891.

Assenheimer, M. & Steinberg, V. 1996 *Europhys. News*, **27**, 143.

Boukari, H., Shaumeyer, J. N., Briggs, M. E. & Gammon, R. W. 1990 Critical speeding up in pure fluids. *Phys. Rev.* A **41**, 2260–2263.

Bravais, P., Zappoli, B. & Mignon, C. 1993 Free convection in the vicinity of the critical point. 14th IAF Congress, Graz, Austria.

Carlès, P. 1995 Etude de l'effet piston et des phénomènes thermo-acoustiques dans les fluides supercritiques. PhD dissertation, Institut National Polytechnique, Toulouse, France.

Carlès, P. & Ugurtas, B. 1999 The onset of free convection near the liquid-vapour critical point. Part I: Stationary initial state. *Physica* D **126**, 69–82.

Chandrasekar, S. 1961 *Hydrodynamic and Hydromagnetic Stability*. Clarendon Press, Oxford.

Garrabos, Y., Bonetti, M., Beysens, D., Perrot, F., Fröhlich, T., Carlès, P. & Zappoli, B. 1998 Relaxation of a supercritical fluid after a heat pulse in absence of gravity effects. *Phys. Rev.* E **57**, 5665–5681.

Gilly, B., El Ganaoui, M., Raspo, I., Amiroudine, S., Larroudé, P., Bontoux, P. & Zappoli B. 1999 Etude numérique des instabilités convectives dans une couche de fluide supercritique avec effet de distance au point critique. 14ème Congrès Français de Mécanique, Proc. 862/1–6, September. Toulouse, France.

Gitterman, M. 1978 Hydrodynamics of fluids near a critical point, approach. *Rev. Mod. Phys.* **50**, 85–106.

Gitterman, M. & Steinberg, V. A. 1970*a* Criteria of occurrence of free convection in a compressible viscous heat-conducting fluid. *J. Appl. Math. Mech.* (305–311) *USSR P.M.M.*, **34**(2), 325–331.

Gitterman, M. & Steinberg, V. A. 1970*b* Criteria for the commencement of convection in a liquid close to the critical point. *High Temperature, USSR* **8**(4), 754–759.

Gitterman, M. & Steinberg, V. A. 1972 Establishment of thermal equilibrium in a liquid near the critical point. *High Temperature, USSR* **10**, 501.

Guenoun, P., Beysens, D., Khalil, B., Garrabos, Y., Kammoun, B., Le Neindre, B. & Zappoli, B. 1993 A thermo cycle around the critical point of CO_2 under reduced gravity. *Phys. Rev.* E **47**, 1531–1540.

Jeffreys, H. 1930 *Proc. Camb. Phys. Soc.* **26**, 170.

Kogan, A. B., Murphy, D. & Meyer, H. 1999 Onset of Rayleigh–Bénard convection in a very compressible fluid: ^{3}He near T_c. *Phys. Rev. Lett.* **82**, 4635–4638.

Kurowski, P., Misbah, C. & Tchourkine, S. 1995 Gravitational instability of a fictitious front during mixing of miscible fluids. *Eur. Phys. Lett.* **29**, 309–314.

Landau, L. D. & Lifschitz, E. M. 1959 *Fluid Mechanics*, vol. 6. Pergamon.

Larroudé, L., Amiroudine, S., Bontoux, P. & Zappoli, B. 1996 Mechanisms of the onset of Rayleigh–Bénard instabilities for a near critical fluid, 31st COSPAR Scientific Assembly, Birmingham, July 1996 (see in *Advances in Space Research*, vol. 22, 8, pp. 1249–1252, 1998, Pergamon).

Larroudé, P., Gilly, B., Amiroudine, S., Zappoli, B. & Bontoux, P. 1997 Instabilités de Rayleigh–Bénard dans un gaz à proximité du point critique. *8ème Journées Internationales de Thermique, Proceedings*, vol. 2, pp. 69–78, July. Marseille, France.

Moldover, M. R., Sengers, J. V., Gammon, R. W. & Hocken, R. J. 1979 Gravity effects in fluids near the gas–liquid critical point. *Rev. Mod. Phys.* **51**, 79–99.

Nitsche, K. & Straub, J. 1987 The critical hump of Cv under microgravity, results from the D-Spacelab experiment 'Wärmekapazität'. *Proceedings of the 6th European Symp. on Material Sci. under Microgravity Conditions*, ESA SP-256, pp. 109–116.

Normand, C., Pomeau, Y. & Velarde, M. G. 1977 Convective instability: a physicist's approach. *Rev. Mod. Phys.* **49**, 581–624.

Onuki, A., Hao, H. & Ferrel, R. A. 1990 Fast adiabatic equilibration in a single-component fluid near the liquid–vapor critical point. *Phys. Rev.* A **41**, 2256–2259.

Paolucci, S. 1982 On the filtering of sound from the Navier–Stokes equations. *Rep. SAND* 82–8257, December. Sandia National Lab., USA.

Patankar, S. V. 1980 *Numerical Heat Transfer and Fluid Flow*. Hemisphere, New York.

Raspo, I., Gilly, B., Amiroudine, S., Bontoux, P. & Zappoli, B. 1999 Simulation of convective instabilities inside a supercritical fluid layer under Rayleigh–Bénard configuration. *J. Chim. Phys.* **96**, 1059–1065.

Spiegel, E. A. 1965 Convective instability in a compressible atmosphere. I. *Astrophys. J.* **141**, 1068.

Zappoli, B. 1992 The response of a nearly supercritical pure fluid to a thermal disturbance. *Phys. Fluids* A **4**, 1040–1048.

Zappoli, B., Amiroudine, S., Carlès, P. & Ouazzani, J. 1996 Thermoacoustic and buoyancy-driven transport in a square side-heated cavity filled with a near-critical fluid. *J. Fluid Mech.* **316**, 53–72.

Zappoli, B., Amiroudine, S. & Gauthier, S. 1997 Instabilité gravitationnelle dans un fluide supercritique pur. *C. R. Acad. Sci. Paris* **325** (IIb), 1–6.

Zappoli, B., Bailly, D., Garrabos, Y., Le Neindre, B., Guenoun, P. & Beysens, D. 1990 Anomalous heat transport by the piston effect in supercritical fluids under zero gravity. *Phys. Rev.* A **41**, 2224–2267.

Zappoli, B. & Carlès, P. 1995 The thermo-acoustic nature of the critical speeding up. *Eur. J. Mech.* B/*Fluids* **14**, 41–65.

Zappoli, B. & Durand-Daubin, A. 1994 Heat and mass transport in a near supercritical fluid. *Phys. Fluids* **6**, 1929–1936.

Zappoli, B., Jounet, A., Amiroudine, S. & Mojtabi, K. 1999 Thermoacoustic heating and cooling in hypercompressible fluids in the presence of a thermal plume. *J. Fluid Mech.* **388**, 389–409.

Zhong, F. & Meyer, H. 1995 Density equilibration near the liquid–vapor critical point of a pure fluid: single phase $T > T_c$. *Phys. Rev.* E **51**, 3223–3241.